IEEE Access
Multidisciplinary | Rapid Review | Open Access Journal

Received August 12, 2017, accepted September 9, 2017, date of publication September 14, 2017,
date of current version October 12, 2017.

Digital Object Identifier 10.1109/ACCESS.2017.2752238

A Multi-Carrier *M*-Ary Differential Chaos Shift Keying System With Low PAPR

TINGTING HUANG[1], LIN WANG[1], (Senior Member, IEEE), WEIKAI XU[1], (Member, IEEE), AND GUANRONG CHEN[2], (Fellow, IEEE)

[1]College of Information Science and Technology, Xiamen University, Fujian 361005, China
[2]Department of Electronic Engineering, City University of Hong Kong, Hong Kong

Corresponding author: Lin Wang (wanglin@xmu.edu.cn)

This work was supported in part by the NSF of China under Grant 61671395, and in part by the Hong Kong Research Grants Council under the GRF Grant CityU 11208515.

ABSTRACT An improved multi-carrier *M*-ary differential chaos shift keying (MM-DCSK) system is presented, where differential modulation and demodulation are carried out across multiple carriers in the frequency domain, so channel estimation is not needed. For one data frame transmission, only one non-information-bearing reference sub-carrier signal is required, and the reference of each information-bearing sub-carrier is its previous sub-carrier signal, thus high energy efficiency is attained. If channel response changes during a frame period, the time diversity is achieved. In addition, the peak-to-average power ratio (PAPR) is considered, and it is found that adjacent symbols with a large Euclidean distance achieve a low PAPR. Accordingly, a low-complexity PAPR reduction algorithm is proposed based on symbol-interleaving with only one inverse fast Fourier transform processor. The simulation results demonstrate that the system with the proposed algorithm dramatically reduces the PAPR. Analytical bit-error-rate expressions are derived and verified by simulations over additive white Gaussian noise and multi-path fading channels.

INDEX TERMS Multi-carrier system, DCSK, complexity, PAPR reduction algorithm.

I. INTRODUCTION

Chaotic signals are non-periodic, random-like, spread-spectrum signals from nonlinear dynamical systems. Chaotic modulations demonstrate many attractive features, including simple transceiver circuits, high robustness to multi-path degradation and good communication security. Therefore, various modulation and demodulation schemes have been suggested [1].

Without the demand of channel estimation and chaotic synchronization, non-coherent chaos-based schemes have attracted a lot of interests. As a kind of non-coherent systems, the differential chaos shift keying (DCSK) system [2] and its constant power version named frequency-modulated DCSK (FM-DCSK) system [3] have been proposed, which have simple implementation with excellent performance. In recent years, several DCSK-based systems with simple transceivers demonstrate excellent performances when being combined with conventional communication techniques, such as multiple-input multiple-output (MIMO) settings, cooperative communications, coding, coexistence and space-time block coding (STBC) [4]–[7]. Particularly, DCSK-based systems have been proposed as a candidate of digital modulation for wireless sensor networks (WSN) and some DCSK/FM-DCSK-based UWB systems are proved feasible for wireless personal area networks (WPAN) [8]–[11].

However, the main drawback of the DCSK systems is that half of the bit duration is spent on sending non-information-bearing reference samples, which leads to low data rate and energy efficiency. Much effort has been devoted to overcoming the drawback. In single-carrier DCSK systems, it is effective to improve the data rate by employing Walsh codes (i.e., [13]–[17]). Another method for increasing data rate is using 2-d constellation mappings. In [18], *M*-ary symbols are formed by using conventional sine and cosine waves as basis functions. Both the square-constellation-based *M*-ary DCSK [19] and the multi-resolution *M*-ary DCSK systems [20] employ the Hilbert transform to produce two orthogonal chaotic signals as basis functions.

The multi-carrier modulation is chosen in this paper since it is an alternative approach permitting high data rate, which requires no delay circuits at both the transmitter and the receiver. In the multi-carrier DCSK (MC-DCSK) system [21], the reference and information-bearing chaotic

signals are modulated on separated frequency bands. It requires the frequency-domain channel responses to be the same on all the sub-carriers. The multi-carrier chaos shift keying (MC-CSK) system [22] employs sine and cosine waves to transmit reference and information signals, respectively, where the energy efficiency is not improved comparing with the DCSK system. The OFDM-based DCSK system [23] reduces the hardware complexity by employing FFT/IFFT, with one-bit chaotic chips spread over sub-carriers in the frequency domain, where it requires that the reference OFDM symbol and the following information-bearing OFDM symbols have the same channel responses. Obviously, the system is designed for very slow fading channels, such as block fading channels. To fully use frequency- and time-domain spreading, the multiuser orthogonal frequency division multiplexing (OFDM)-based DCSK system (MU OFDM-DCSK) is proposed [24], where one-bit chaotic chips are spread in the time domain. The pilot signals are inserted instead of using channel estimation. Apparently, more pilot signals are required when the system suffers a severe frequency selective fading, thus the energy efficiency is reduced. Therefore, the good performance of MU OFDM-DCSK is at the cost of low energy efficiency.

To further improve the MU OFDM-DCSK system, in this paper, an M-ary multi-carrier DCSK system is designed and validated. Inspired in [25] and [26], the adjacent sub-carriers with highest correlation are employed in this paper. To achieve a high energy efficiency, each chaotic sub-carrier signal is used as the reference for its next adjacent sub-carrier signal. Therefore, only one non-information-bearing chaotic signal is required. Moreover, the system is applicable to M-ary transmission. Here, M-ary DCSK symbols are formed by employing a sine and a cosine wave as basis functions. Furthermore, the frequency responses over every two adjacent sub-carriers are assumed to be approximately equal. It is noteworthy that approximate equality is not transitive, that is, if $x \approx y$, $y \approx z$, it may not imply that $x \approx z$. Therefore, the assumption in the paper does not require all the given sub-carriers have same channel gains. In addition, a multi-carrier signal, especially OFDM signal, suffers from a high PAPR, which is a big challenge for transmitters [27]. However, to the best of our knowledge, there are very few articles considering PAPR of multi-carrier DCSK systems. In this paper, a low-complexity symbol-interleaving (SI) PAPR-reduction algorithm utilizing chaos characteristics is proposed. Comparing with the traditional SI technique, the proposed algorithm requires only one IFFT operator, which reduces the computational complexity.

The contributions of this work are summarized as follows.

1) A multi-carrier M-ary DCSK system is proposed, where chaotic chips are spread in the time domain as the MU OFDM-DCSK system, so that if the channel response changes during one data frame transmission, the time diversity is achieved. Differing from the MU OFDM-DCSK system using pilot signals, the proposed system employs adjacent sub-carriers with high correlation, where each modulated sub-carrier chaotic signal is the reference for its next adjacent sub-carrier signal. Thus, only one non-information sub-carrier signal is required instead of a number of pilot signals, thereby achieving good energy efficiency. In addition, the information-bearing signal and its reference are allocated at adjacent sub-carriers on a minimum frequency interval. As a result, the proposed system is robust to multi-path effect and Doppler shift.

2) The generalized analytical BER expressions are derived and verified by computer simulations over AWGN and multi-path fading channels.

3) A low-complexity PAPR-reduction algorithm is proposed.

4) The system is applicable for M-ary transmission.

The rest of the paper is organized as follows: Section II presents the system model of the MM-DCSK scheme; Section III derives the BER expressions; Section IV demonstrates the simulation results, while Section V summarizes the findings with conclusions.

II. SYSTEM MODEL OF THE MM-DCSK SCHEME

The MM-DCSK system to be studied is shown in Fig.1. This system is able to achieve a high data rate and a good energy efficiency. In addition, it benefits from time diversity without using complex channel estimators.

A. THE MM-DCSK TRANSMITTER

In the following discussion the guard band is not considered, for the interest here is to utilize the properties of chaotic signals to design a simple M-ary scheme. Assume that the inter symbol interference (ISI) can be eliminated by inserting a cyclic prefix. For simplicity, the cyclic prefix is not expressed by mathematical equations. As assumed in [20], the chaotic signal are normalized, such that $\sum_{i=1}^{\beta} c_i^2 = 1$. Due to the superior performance over other chaotic maps, the logistic map $c_{i+1} = 1 - 2c_i^2, i \in \mathbb{Z}^+$, is employed to generate chaotic sequences $\mathbf{c} = (c_1, c_2, \cdots, c_\beta)$ with zero mean and unit variance, i.e., $\mathrm{E}(c_i) = 0$, $\mathrm{E}(c_i^2) = 1$.

At the transmitter side, the serial data symbol sequence $\mathbf{d}$ takes values from a normalized M-ary phase-shift keying (PSK) modulation constellation $\mathcal{C}$, which is $\mathbf{d} = \{d_1, d_2, \cdots, d_N\}, d_n = a_n + jb_n, a_n^2 + b_n^2 = 1, d_1 = 1 + 0j, 1 \le n \le N, j = \sqrt{-1}$. The symbol sequence is firstly converted to sub-streams by a serial-to-parallel (S/P) converter.

Let d_n be the information symbol transmitted on the n-th sub-carrier. Specially, the first sub-stream d_1, spread by the original chaotic sequence $\mathbf{c}$, becomes $\mathbf{S}_1$ and is assigned to the first sub-carrier as the reference signal. For the second sub-carrier, the information sub-carrier signal $\mathbf{S}_n$ is formed by its previous sub-carrier signal $\mathbf{S}_{n-1}$ and the symbol d_n. Thus, the complex-valued n-th sub-carrier signal can be given in a vector form, as

$$\begin{aligned}\mathbf{S}_n &= \sqrt{E_s^{sub}} d_n \mathbf{S}_{n-1} \\ &= \sqrt{E_s^{sub}} d_1 \cdot d_2 \cdots d_n \mathbf{c} \\ &= (S_{1,n}, S_{2,n}, \cdots, S_{\beta,n}),\end{aligned} \tag{1}$$

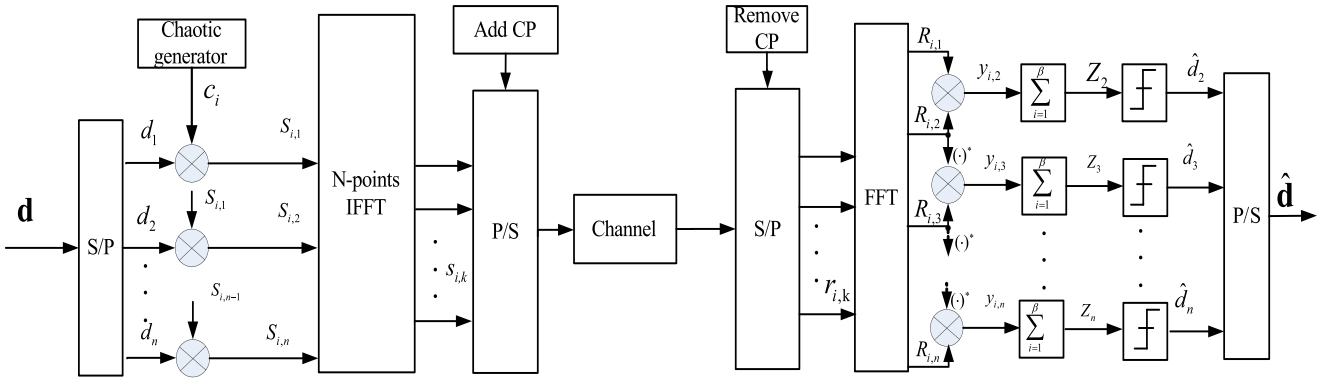

FIGURE 1. The transceiver of the MM-DCSK system.

where $\mathbf{S}_1 = \sqrt{E_s^{sub}}\mathbf{c}$, $E_s^{sub} = \frac{(N-1)E_s}{N}$ denotes the average energy of each sub-carrier and E_s is the symbol energy.

Note that $\mathbf{S}_n$ is a new complex chaotic signal, correlating $\mathbf{S}_n$ with $\mathbf{S}_{n-1}$, such that $\mathbf{S}_n \times \mathbf{S}_{n-1}^* = E_s^{sub} d_n \cdot |d_{n-1}| \cdot |d_{n-2}| \cdots |d_1| \cdot (\sum_{i=1}^{\beta} c_i^2)$, where $(\cdot)^*$ denotes the Hermitian transpose. It is clear that the symbol d_n can be recovered easily by slicing the output.

Here, consider N sub-carriers for each multi-carrier symbol with symbol duration T_s. An N-point IFFT is employed to generate time-domain symbols. Therefore, for the discrete-time representation, the k-th ($1 \le k \le N$) sample of the i-th ($i = 1, 2, \ldots, \beta$) multi-carrier symbol is expressed as

$$s_{i,k} = \frac{1}{\sqrt{N}} \sum_{n=1}^{N} S_{i,n} e^{j2\pi nk/N}. \tag{2}$$

Then, a cyclic prefix is added to the beginning of each multi-carrier symbol so as to resist the ISI and, finally, the transmitted signal is converted from parallel to serial (P/S) before transmitting.

B. THE MM-DCSK NON-COHERENT RECEIVER

On the receiver side, a reverse operation is performed to convert the received serial signal to parallel. Then, the cyclic prefix is removed. The k-th sample of the i-th received time-domain multi-carrier symbol is

$$r_{i,k} = s_{i,k} \otimes h_{i,k} + \eta_{i,k}. \tag{3}$$

Assume that the channel is a Rayleigh multipath fading channel with L paths. Then, $h_{i,k}$ is the discrete-time equivalent impulse in the multipath channel, i.e, $h_{i,k} = \sum_{l=0}^{L-1} \alpha_{i,l} \delta(\tau - \tau_{i,l})$, with $\alpha_{i,l}$ being the independent zero-mean complex Gaussian random variable of the l-th path having variance $\sigma_{i,l}^2$; $\otimes$ denotes the convolution operation; $\tau_{i,l}$ is the delay time of the l-th path and $\eta_{i,k}$ is the k-th sample of the complex Gaussian noise with zero mean and variance N_0. The parallel signals are fed into the FFT processor to convert signals back into the frequency domain. Thus, the n-th sub-carrier signal is presented by

$$R_{i,n} = S_{i,n} H_{i,n} + N_{i,n}, \tag{4}$$

where $H_{i,n} = \frac{1}{\sqrt{N}} \sum_{l=0}^{L-1} \alpha_{i,l} e^{-j2\pi f_n \tau_{i,l}}$ is the frequency response of $h_{i,n}$. Without loss of generality, normalize the variance of the channel gain on each sub-carrier, where the absolute value of $H_{i,n}$ is Rayleigh-distributed with the probability density function (PDF) $f(\alpha) = 2\alpha e^{(-\alpha^2)}$. According to the auto-coherent detector, the output of the n-th ($n > 1$) multiplier is

$$\begin{aligned} y_{i,n} &= R_{i,n} R_{i,n-1}^* \\ &= \left(H_{i,n} S_{i,n} + N_{i,n}\right)\left(H_{i,n-1}^* S_{i,n-1} + N_{i,n-1}^*\right) \\ &= H_{i,n} H_{i,n-1}^* S_{i,n} S_{i,n-1} + H_{i,n} S_{i,n} N_{i,n-1}^* \\ &\quad + H_{i,n-1}^* S_{i,n-1} N_{i,n} + N_{i,n} N_{i,n-1}^*. \end{aligned} \tag{5}$$

After the β-th OFDM symbol is received at the receiver, the output of the n-th ($n > 1$) integrator block becomes

$$Z_n = \sum_{i=1}^{\beta} y_{i,n}. \tag{6}$$

Note that the demodulation for each sub-carrier symbol is independent of each other. Therefore, catastrophic errors will not appear in this system.

C. DECISIONS

The decision is taken on the phase of the complex value $Z_n = Z_n^a + jZ_n^b$, i.e., $w = \arctan(Z_n^b / Z_n^a)$. This phase is then adopted for decoding the bit streams, i.e., identifying the most likely transmitted phase θ, so that the information bits can be recovered corresponding to this θ.

D. CORRELATION FUNCTION BETWEEN SUB-CARRIERS OVER AN MULTI-PATH FADING CHANNEL

Since the transceiver here is based on the high correlation of adjacent sub-carriers, it is necessary to investigate the effects of multipath fading channels on correlation. The frequency

response of the n-th subcarrier after N-point IFFT is

$$H_n = \frac{1}{\sqrt{N}} \sum_{l=0}^{L-1} \alpha_l e^{-j2\pi n\tau_l/NT}, \tag{7}$$

where T is the sample period. The frequency correlation function between any two sub-carriers Δn [25] is given by

$$C_{\Delta n} = E\{H_n H_{n+\Delta n}^*\} = \frac{1}{N} \sum_{l=0}^{L-1} {\sigma_l}^2 e^{j2\pi\,\Delta n\tau_l/NT}. \tag{8}$$

From Eq. (8), it follows that the inter-subcarrier correlation reduces when L or τ_l is increased. The loss of correlation has a negative impact on performance. Nevertheless, the channel gains of adjacent (i.e., $\Delta n = 1$) sub-carriers considered in this paper maintain the highest correlation on various frequency intervals.

E. ANALYSIS OF ENERGY EFFICIENCY AND SPECTRAL EFFICIENCY

1) ENERGY EFFICIENCY

The data-energy to symbol-energy (DS) ratio is defined to be the uniform energy efficiency for the following three systems in comparison. For the conventional DCSK system,

$$DS = \frac{1}{2}. \tag{9}$$

For the MU OFDM-DCSK system,

$$DS = \frac{N_s}{N_s + N_{cp} + N_{re}}, \tag{10}$$

where N_s denotes the number of transmitted symbols, N_{cp} is the number of sub-carriers allocated to transmit the cyclic prefix and $N_{re} \geq 3$ is the number of pilots. For the proposed MM-DCSK system,

$$DS = \frac{N_s}{N_s + N_{cp} + 1}. \tag{11}$$

It is easy to see that the energy efficiency of the proposed system is better than both the conventional DCSK and the MU OFDM-DCSK systems.

2) SPECTRAL EFFICIENCY

Obviously, the ratio of bandwidth efficiency of MM-DCSK to MU OFDM-DCSK is $\frac{\log_2 M \times N_s}{N_s - N_{re} + 1}$. One can observe that the spectral efficiency of the proposed MM-DCSK system is superior to that of MU OFDM-DCSK systems.

III. PERFORMANCE ANALYSIS

In this section, the analytical BER expressions of the MM-DCSK system over AWGN and multipath Rayleigh fading channels are derived.

To simplify the analysis, assume that the maximum channel time delay τ_{max} is much shorter than the multi-carrier symbol duration (T_s), i.e., $\tau_{max} \ll T_s$, so the channel can be seen by each sub-carrier as flat. Due to the high correlation of the adjacent sub-carriers, assume also $H_{i,n} \approx H_{i,n-1}$. In addition, assume that during the time interval Δt, the channel impulse response remains constant, i.e., $\Delta t = \lceil \frac{\beta T_s}{P} \rceil$, where $\beta = pP$, P is the number of independent fading blocks of the channel in duration βT_s, $p \in \mathbb{Z}^+$, and $\lceil \cdot \rceil$ is the ceiling operator. Since all frame signals with β multi-carrier symbols are independent of each other, one can simply focus on the first frame signal for analysis.

A. DERIVATION OF BER EXPRESSIONS

Since β multi-carrier symbols are collected before demodulation as mentioned in Section II-B, it is essential to investigate the BER performances with different numbers of channel blocks (P).

Firstly, substituting Eq. (1) and Eq. (5) into Eq. (6), the output of the n-th ($n > 1$) integrator Z_n can be obtained with a generalized expression in terms of P, as

$$\begin{aligned} Z_n &= E_s^{sub} d_n \sum_{i=1}^{\frac{\beta}{P}} \sum_{p=1}^{P} \left|H_{p,n}\right|^2 c^2_{\frac{\beta}{P}(p-1)+i} \\ &\quad + \sqrt{E_s^{sub}} \sum_{i=1}^{\frac{\beta}{P}} \left(\prod_{m=1}^{m=n} d_m \sum_{p=1}^{P} H_{p,n} N^*_{i,n-1} c_{\frac{\beta}{P}(p-1)+i} \right. \\ &\quad \left. + \sum_{p=1}^{P} H^*_{p,n-1} N_{i,n} c_{\frac{\beta}{P}(p-1)+i} \right) + \sum_{i=1}^{\beta} N_{i,n} N^*_{i,n-1} \\ &= Z_n^a + jZ_n^b. \end{aligned} \tag{12}$$

It is easy to verify that the decision variables Z_n^a and Z_n^b are independent Gaussian variables, so the expectations and variances of Z_n^a and Z_n^b can be obtained, as

$$\mathrm{E}(Z_n^a) = \frac{E_s^{sub}}{P} a_n \sum_{p=1}^{P} \left|H_{p,n}\right|^2, \tag{13}$$

$$\mathrm{E}(Z_n^b) = \frac{E_s^{sub}}{P} b_n \sum_{p=1}^{P} \left|H_{p,n}\right|^2, \tag{14}$$

$$\mathrm{var}(Z_n^a) = \frac{E_s^{sub}}{P} N_0 \sum_{p=1}^{P} \left|H_{p,n}\right|^2 + \beta \frac{(N_0)^2}{2}, \tag{15}$$

$$\mathrm{var}(Z_n^b) = \frac{E_s^{sub}}{P} N_0 \sum_{p=1}^{P} \left|H_{p,n}\right|^2 + \beta \frac{(N_0)^2}{2}. \tag{16}$$

It is interesting to see that Z_n^a and Z_n^b have the same variance. Denote $m_1 = \frac{E_s^{sub}}{P} a_n \sum_{p=1}^{P} \left|H_{p,n}\right|^2$, $m_2 = \frac{E_s^{sub}}{P} b_n \sum_{p=1}^{P} \left|H_{p,n}\right|^2$, $\sigma^2 = \frac{E_s^{sub}}{P} N_0 \sum_{p=1}^{P} \left|H_{p,n}\right|^2 + \beta \frac{(N_0)^2}{2}$ and the symbol energy to noise ratio $\gamma_s^n = E_s^{sub} \sum_{p=1}^{P} \left|H_{p,n}\right|^2 / N_0$.

Then, the joint PDF of Z_n^a and Z_n^b is given by

$$p(Z_n^a, Z_n^b|H_{p,n}) = \frac{1}{2\pi\sigma^2}\exp\left(-\frac{(Z_n^a - m_1)^2 + (Z_n^b - m_2)^2}{2\sigma^2}\right). \quad (17)$$

Consequently, the polar coordinate transformation of the decision vector (Z_m^a, Z_m^b) is given by

$$\begin{cases} V = \sqrt{Z_n^{a2} + Z_n^{b2}}, \\ \Omega = arctan(Z_n^b/Z_n^a). \end{cases} \quad (18)$$

Equation (17), when expressed in polar coordinates, can be rewritten as

$$p_{V,\Omega}(v, w|H_{p,n}) = \frac{v}{2\pi\sigma^2}\times\exp\left(-\frac{v^2-2v(m_1\cos w+m_2\sin w)+m_1^2+m_2^2}{2\sigma^2}\right). \quad (19)$$

Integrating it over v, the instant marginal pdf of Ω is obtained as

$$\begin{aligned} p_\Omega(w|H_{p,n}) &= \int_0^{+\infty} p_{V,\Omega}(v, w)dv \\ &= \int_0^{+\infty} \frac{v}{2\pi\sigma^2} \\ &\quad \times \exp\left(-\frac{v^2 - 2v(m_1\cos w + m_2\sin w) + m_1^2 + m_2^2}{2\sigma^2}\right) \mathrm{d}v. \end{aligned} \quad (20)$$

Due to the M-PSK modulation, $\cos\theta = a_n$, $\sin\theta = b_n$. Substituting them into Eq. (20) yields

$$\begin{aligned} p_\Omega(w|H_{p,n}) &= \int_0^{+\infty} \frac{v}{2\pi\sigma^2} \\ &\quad \times \exp\left(-\frac{v^2 - 2vG(\cos\theta\cos w + \sin\theta\sin w) + G^2}{2\sigma^2}\right) \mathrm{d}v \\ &= \int_0^{+\infty} \frac{v}{2\pi\sigma^2} \times \exp\left(-\frac{v^2 - 2vG\cos(w-\theta) + G^2}{2\sigma^2}\right) \mathrm{d}v \\ &= \int_0^{+\infty} \frac{v}{2\pi\sigma^2} \times \exp\left(-\frac{v^2 - 2vG\cos\varphi + G^2}{2\sigma^2}\right) \mathrm{d}v, \end{aligned} \quad (21)$$

where φ denotes the phase error between the transmitted and received signals, and $G^2 = m_1^2 + m_2^2$. Let $t = \frac{v}{\sigma}$. Then, Eq. (21) can be rewritten as

$$\begin{aligned} p(\varphi|H_{p,n}) &= \int_0^{+\infty} \frac{t}{2\pi} \times \exp\left(-\frac{t^2 - 2t\frac{G}{\sigma}\cos\varphi + \frac{G^2}{\sigma^2}}{2}\right) \mathrm{d}t \\ &= \int_0^{+\infty} \frac{t}{2\pi} \times \exp\left(-\frac{t^2 - 2t\rho\cos\varphi + \rho^2}{2}\right) \mathrm{d}t \\ &= \int_0^{+\infty} \frac{t}{2\pi} \times \exp\left\{-\frac{1}{2}\left[(t-\rho\cos\varphi)^2 + \rho^2\sin\varphi^2\right]\right\} \mathrm{d}t \\ &= \exp\left(-\frac{1}{2}\rho^2\sin\varphi^2\right) \times \int_0^{+\infty} \frac{t}{2\pi}\exp\left[-\frac{(t-\rho\cos\varphi)^2}{2}\right] \mathrm{d}t \\ &= \exp\left(-\frac{1}{2}\rho^2\sin\varphi^2\right) \\ &\quad \times \left\{\int_0^{+\infty} \frac{t-\rho\cos\varphi}{2\pi}\exp\left[-\frac{1}{2}(t-\rho\cos\varphi)^2\right] \mathrm{d}t \right. \\ &\quad \left. + \int_0^{+\infty} \frac{\rho\cos\varphi}{2\pi}\exp\left[-\frac{1}{2}(t-\rho\cos\varphi)^2\right] \mathrm{d}t\right\} \\ &= \exp\left(-\frac{1}{2}\rho^2\sin\varphi^2\right) \\ &\quad \times \left[\frac{1}{2\pi}\exp\left(-\frac{1}{2}\rho^2\cos\varphi^2\right) + \frac{\rho\cos\varphi}{\sqrt{2\pi}}\mathrm{Q}(-\rho\cos\varphi)\right], \end{aligned} \quad (22)$$

where $\mathrm{Q}(x) = 1/\sqrt{2\pi}\int_x^\infty \exp(-t^2/2)\mathrm{d}t$, for $x \geq 0$; $\rho = \frac{G}{\sigma}$.

Note that, the absolute value of channel response is Rayleigh-distributed, so $|H_{p,n}|^2$ is chi-square distributed with two degrees of freedom, and γ_s^n is also chi-square distributed. Thus, the symbol error radio (p_e) of the system is given by

$$p_e = \int_{\pi/M}^{\pi}\int_0^{+\infty} p(\varphi|\gamma_s^n)f(\gamma_s^n)\mathrm{d}\gamma_s^{\mathrm{n}}. \quad (23)$$

The BER is $p_b \approx p_e/\log_2(M)$.

B. THE PROPOSED PAPR-REDUCTION ALGORITHM

One of the major disadvantages of OFDM is its high PAPR, which is a great challenge for power amplifiers. The proposed MM-DCSK system also suffers from a high PAPR.

1) SYMBOL-INTERLEAVING PAPR-REDUCTION ALGORITHM

Among all the PAPR reduction techniques, the interleaving technique is considered a good alternative for its similar complexity to the PTS (partial transmit sequence) method with comparable results [28]. The traditional SI technique employs V interleavers to produce permuted sequences from the same information sequence. Then, V IFFT operations are required to generate V time-domain candidate signals. The signal with the lowest PAPR is selected to transmit. It requires the transmitter to store all the permutation indices. The PAPR statistics improve with increasing V; that is, good PAPR is achieved at the cost of a large number of interleavers, which leads to a requirement of powerful processors and vast storage capacities. Therefore, the traditional SI technique is not desirable for low-cost devices.

2) THE PROPOSED PAPR-REDUCTION ALGORITHM

It is demonstrated that repeated data blocks lead to a high PAPR, and adjacent symbols with a large Euclidean distance achieve a low PAPR. The proposed PAPR-reduction algorithm tries to increase adjacent symbols' Euclidean distances by permutation, but whether it could increase the repeated data blocks is not considered. Since the proposed

TABLE 1. The probability of $\lambda_{proposed} < \lambda_{original}$.

	M=4	M=8	M=16	M=32
$N = 64$	0.7047	0.9993	1	1
$N = 128$	0.1554	0.9999	1	1
$N = 256$	0.0004	1	1	1
$N = 512$	0	0.9997	1	1

algorithm permutes symbol sequences in a specific way, so that only one IFFT operator is needed and the candidate permutation indices are not required at the transmitter. Consequently, the computational complexity and memory are reduced. According to such characteristics, the proposed system with the proposed algorithm is very suitable for the hand-held terminal of wireless warehouse. The detailed steps of the proposed PAPR-reduction algorithm are as follows:

Step 1: The incoming Gray-coded data symbols are sorted from small to large according to the decimal equivalent numbers. For instance, assuming that the data symbols array is $\mathbf{d} = \{d_2, d_3, d_4, \cdots, d_N\}$, and d_1 is the reference symbol, a sorted new array is formed, $\mathbf{d}' = \{d'_2, d'_3, d'_4, \cdots, d'_N\}$, where $d'_2 \le d'_3 \le d'_4 \le \cdots \le d'_N$.

Step 2: The array $\mathbf{d}'$ sorted in Step 1 is divided equally into two parts, i.e, $\mathbf{d}''_o = \{d'_2, d'_3, d'_4, \cdots, d'_{\lceil N/2\rceil+1}\}$ and $\mathbf{d}''_e = \{d'_{\lceil N/2\rceil+2}, d'_{\lceil N/2\rceil+3}, \cdots, d'_N\}$. The first part of parameters $\mathbf{d}''_o$ are assigned with odd indexes in the new array $\mathbf{d}''$ and the second part of parameters $\mathbf{d}''_e$ are assigned with even indexes in $\mathbf{d}''$, i.e., $\mathbf{d}'' = \{d'_2, d'_{\lceil N/2\rceil+2}, d'_3, d'_{\lceil N/2\rceil+3}, \cdots, d'_N, d'_{\lceil N/2\rceil+1}\}$. Then, the reordered sequence $\mathbf{d}''' = [d_1, \mathbf{d}'']$ is fed into an S/P converter so as to convert the sub-streams to perform the remaining processes, as shown in Fig.1.

To verify the effectiveness of the algorithm, firstly an upper bound on PAPR is calculated. The intimate relationship between the PAPR and the aperiodic autocorrelation values of the input data sequences is introduced in [29], which is

$$\gamma_{papr} \le 1 + \frac{2}{N}\sum_{k=1}^{N-1}|\rho(k)|, \tag{24}$$

where $\rho(k)$ is the aperiodic autocorrelation coefficients and N is the input sequence length. The upper bound is given by $\lambda = 1 + \frac{2}{N}\sum_{k=1}^{N-1}|\rho(k)|$.

A statistic method is employed to evaluate the probability of $\lambda_{proposed} < \lambda_{original}$, where $\lambda_{proposed}$ denotes the values λ of the reordered sequences, while $\lambda_{original}$ denotes the values λ of the original sequences. Then, 10,000 sets of symbol sequences corresponding to each pair of M and N are generated to calculate $\lambda_{original}$ and $\lambda_{proposed}$. The probability of $\lambda_{proposed} < \lambda_{original}$ is shown in Table 1. It can be seen from Table 1 that, as N increases from 64 to 512, for small M (i.e., $M = 4$), the probability decreases to 0; while for large M (i.e., $M = 32$), the probabilities are very close to 1. This can be explained by the fact that as N increases,

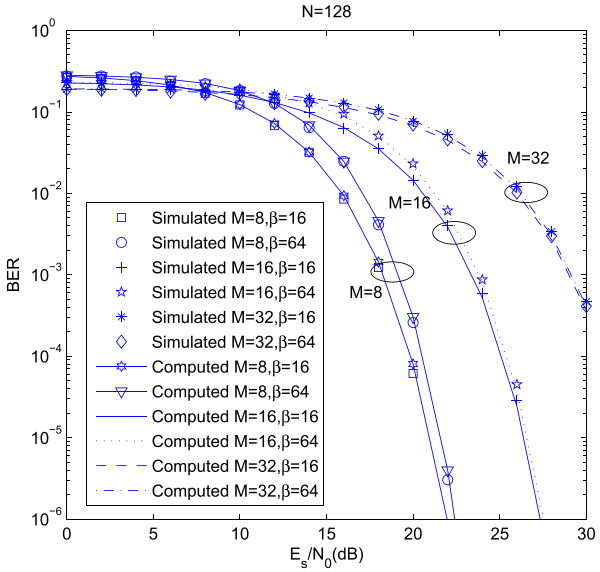

FIGURE 2. Comparisons of computed and simulated BER performances of the MM-DCSK system over an AWGN channel with various values of β and M. The parameters are $\beta = 16, 64$; $M = 8, 16, 32$; $N = 128$.

each symbol belonging to $\{0, 1, \cdots, M-1\}$ is considered to be generated with an equal probability. Thus, for small M the number of times each symbol repeated is large, so the symbol sequence generated with the algorithm increases the number of duplicated symbol blocks; while if M is large, the algorithm effectively separates the repeated symbols.

Another method to verify the effectiveness of the algorithm is to use the complementary cumulative distribution function (CCDF). The CCDF is commonly used to evaluate the probability of PAPR exceeding a certain threshold $PAPR_0$, namely,

$$CCDF(PAPR_0) = \Pr(PAPR > PAPR_0), \tag{25}$$

where PAPR is defined as the ratio of the peak power to the average power within a symbol duration, which is expressed as

$$PAPR = \frac{\max\limits_{1\le k\le N}\left[|s_{i,k}|^2\right]}{E\left[|s_{i,k}|^2\right]}. \tag{26}$$

IV. SIMULATION RESULTS AND DISCUSSION

This section evaluates the performance of the proposed MM-DCSK system over AWGN and multipath Rayleigh fading channels. In all simulations, the sub-carrier spacing is set to be 312.5 KHz and the cyclic prefix duration 0.8 μs.

A. PERFORMANCE EVALUATION OF THE PROPOSED SCHEME

1) AWGN CHANNEL

The effects of the spreading factor β, the number of sub-carriers N and the modulation order M on the BER performance are demonstrated. As can be seen from Fig. 2

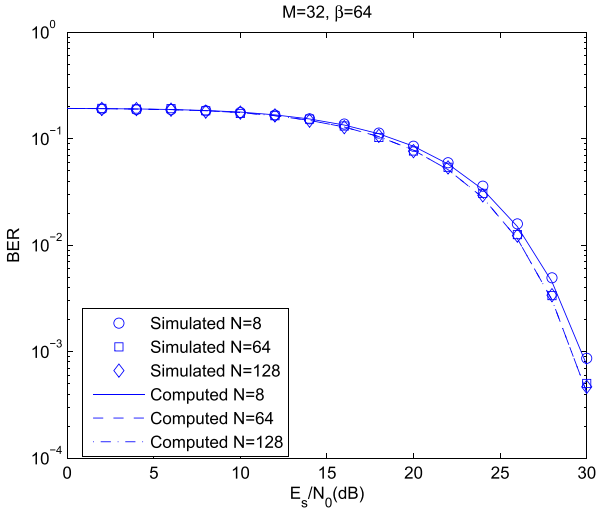

FIGURE 3. Comparisons of computed and simulated BER performances of the MM-DCSK system over an AWGN channel with various values of N. The parameters are $N = 8, 64, 128$; $\beta = 64$; $M = 32$.

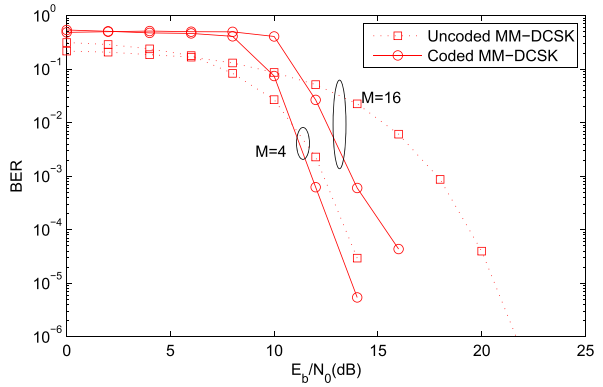

FIGURE 4. Comparisons of simulated BER performances of the uncoded and coded MM-DCSK systems over an AWGN channel. The parameters are $N = 128$; $\beta = 64$; $M = 4, 16$.

and Fig. 3, the theoretical BER curves agree well with the simulated ones.

Fig. 2 shows the effects of β and M on the BER performance. The number of sub-carriers is set to be $N = 128$ and the spreading factor $\beta = 16, 64$ for the cases of $M = 8, 16, 32$, respectively. It can be seen that, differing from other DCSK systems, the β values do not have a significant impact on the BER performance, especially when the modulation order M is large, e.g., $M = 32$. On the contrary, the performance deteriorates sharply as M increases. Hence, it can be concluded that, when M is large, the data rate can be increased by decreasing β.

In Fig. 3, the proportion of the transmitted energy for the reference signal (i.e., $\frac{1}{N}$) on the BER performance is demonstrated. The spreading factor is set to be $\beta = 64$, $M = 32$ and the number of sub-carrier $N = 8, 64, 128$, respectively. It can be seen that, as N increases, the BER performances improve slightly, because the energy consumed for the reference signal can be neglected when N is large, e.g., $N = 64$. The results confirm once again the fact that the system offers a high energy efficiency.

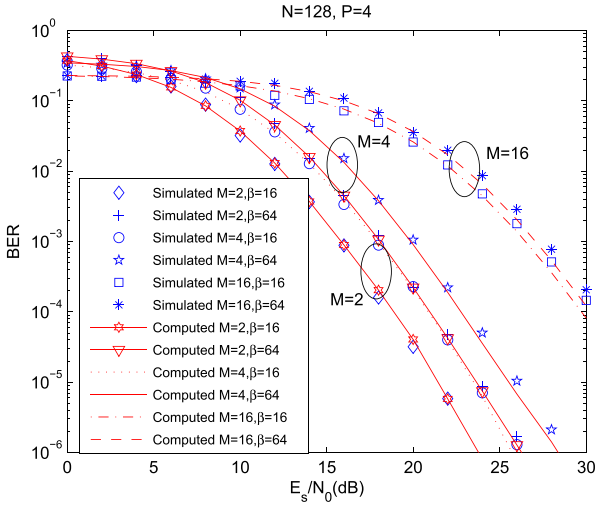

FIGURE 5. Comparisons of computed and simulated BER performances of the MM-DCSK system over a two-path Rayleigh channel with various values of β and M. The parameters are $\beta = 16, 64$; $M = 2, 4, 16$, $N = 128$, $P = 4$.

In Fig. 4 shows the comparisons of simulated BER performances of the uncoded and coded MM-DCSK systems. The simulation parameters are set to be $N = 128$, $\beta = 64$, $M = 4, 16$. In the coded cases, the convolutional code with a rate of $\frac{1}{2}$, constraint length of 7 and a soft-decision Viterbi decoder is employed. It can be seen that the coded MM-DCSK system improves the BER performances greatly, especially when M is large, i.e., $M = 16$.

2) SIMPLE TWO-PATH RAYLEIGH FADING CHANNEL

To further verify the accuracy of the analysis over multipath channels, the BER performances over a two-path Rayleigh fading channel with an equal average power gain ($L = 2, \mathrm{E}[\alpha_l^2] = 1/2$) are evaluated, where the maximum delay is $\tau_{max} = 0.025\mu s$.

Fig. 5 compares the analytical BERs and the simulation results of the proposed system with various M and β. The simulation parameters are set to be $N = 128$, $P = 4$, $\beta = 16, 64$, and $M = 2, 4, 16$, respectively. It can be seen that the theoretical BER curves agree well with the simulated ones. Furthermore, similar conclusions are reached as Fig. 2 regarding the impacts of M and β on the performances.

Fig. 6 demonstrates the BER performance due to the effects of different times interval $\Delta t = \lceil \frac{\beta T_s}{P} \rceil$. Parameters are set to be $N = 128$, $\beta = 64$, $P = 1, 8$ and 64, respectively. One can observe that there is an excellent match between analytical and simulation BERs. More importantly, in a frame period, the sooner the channel changes (P increases), the better the BER performance of the system gains. As mentioned before, each data symbol is spread by a chaotic sequence with β chips. Then, the β chips are transmitted by β multi-carrer symbols. If these β multi-carrier symbols traverse through P independent channels during one transmission, the demodulation process of one data symbol can be considered as an equal gain combining (EGC) with P independent channel coefficients. Therefore, the time diversity is obtained, thus the performance is improved.

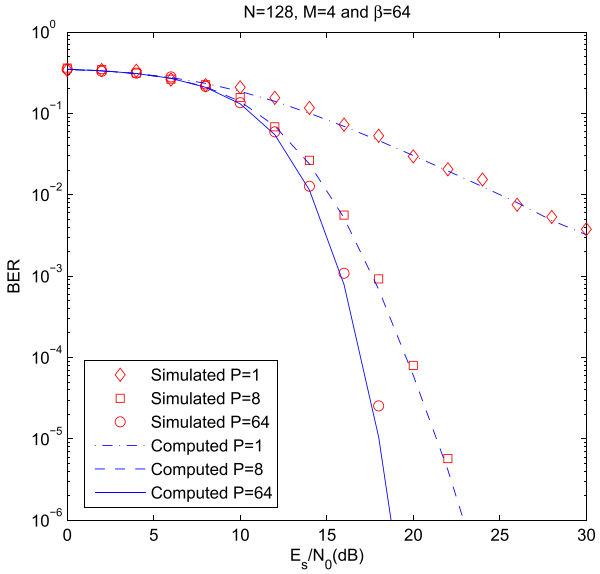

FIGURE 6. Comparisons of computed and simulated BER performances of the MM-DCSK system over a two-path Rayleigh channel with various P. The parameters are $P = 1, 8, 64$, $N = 128$, $\beta = 64$.

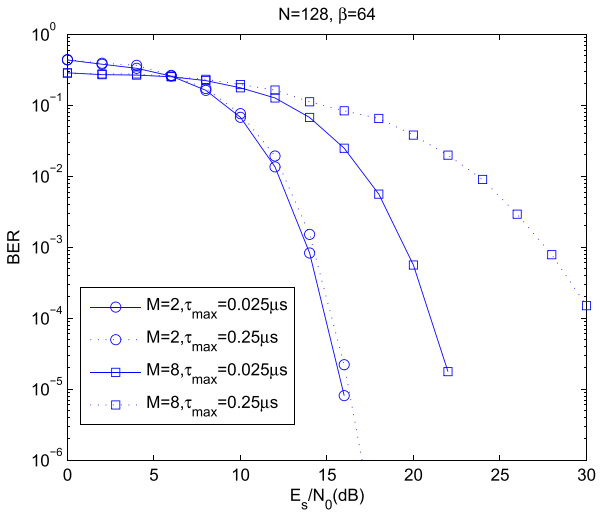

FIGURE 7. BER performances of the MM-DCSK system with various τ_{max}. $P = \beta = 64$, $\tau_{max} = 0.025\mu s$ and $0.25\mu s$, respectively.

In Fig. 7, the impact of sub-carriers correlation on performance is visualized. As mentioned in Section II-D, the sub-carriers correlation reduces as τ_{max} increases. The τ_{max} is set to be $\tau_{max} = 0.025\mu s$ and $\tau_{max} = 0.25\mu s$, respectively, with $M = 2, 8$. One can observe that as the sub-carrier correlation is weakened, the performance of large M (i.e., $M = 8$) deteriorates sharply, while for small M (i.e., $M = 2$) the performance changes slightly. This can be explained that the amplitude and phase of adjacent sub-carriers vary greatly due to the weakened correlation, but the system with large M is sensitive to phase shift, so the performance is not desirable.

3) ITU CHANNEL MODEL FOR INDOOR OFFICE

To further justify the applicability of the proposed system, the ITU channel model for indoor office (Channel A) with variation of Doppler shift is employed to evaluate the performances.

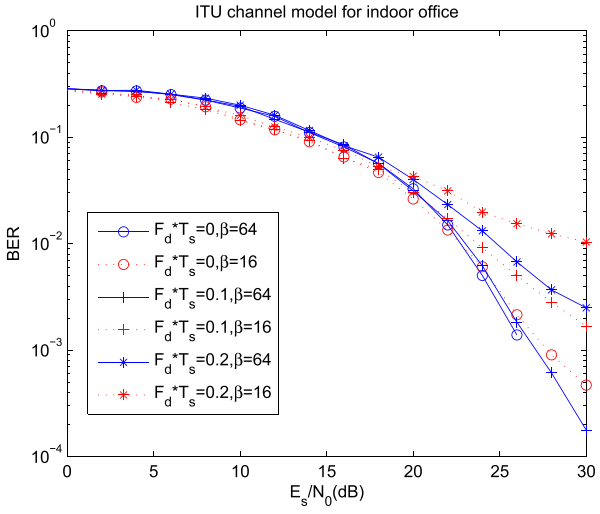

FIGURE 8. BER performances of the MM-DCSK system over ITU channel model for indoor office (Channel A), with $M = 8$, $\beta = 16, 64$.

In Fig. 8, the parameters are $M = 8$, $N = 128$, $\beta = 16, 64$, respectively. It is shown that the proposed MM-DCSK system works properly in the typical frequency selective channel and it is robust to Doppler shift. In addition, it is observed that the system with a larger β (i.e., $\beta = 64$) is more robust to Doppler shift than a smaller one (i.e., $\beta = 16$).

B. PAPR EVALUATION OF THE PROPOSED ALGORITHM

In order to verify the feasibility of the proposed PAPR-reduction algorithm, the CCDF curves are displayed. In Fig. 9, the number of sub-carriers is set to be $N = 64, 512$, respectively, for the cases of $M = 4, 8, 16, 32$, and $\beta = 64$. One can observe that the system with the proposed algorithm having a proper combination of M and N is able to achieve a low CCDF for given PAPRs. Specifically, when $N = 64$ at the probability of 10^{-4}, the PAPR of the proposed algorithm reduces 3.5 dB for $M = 16$, and 1 dB for $M = 8$, respectively. However, when $N = 512$, the PAPR of the proposed algorithm reduces 2 dB for $M = 16$, while it increases 3dB for $M = 8$. That shows, at a given CCDF for large N (e.g., $N = 512$), a large M is more proper than a small one. It is demonstrated that repeated data blocks lead to a high PAPR. For large N, each symbol belonging to $\{0, 1, \cdots, M-1\}$ is considered to be generated with an equal probability. Thus, for small M the number of times each symbol repeated is large, unfortunately the data sequence with the proposed PAPR reduction algorithm further increases the number of duplicated symbol blocks; while if M is large, the algorithm significantly separates the repeated symbols. Therefore, when N is large, it is better to choose a large M; for small M, a small N is required. Accordingly, an optimal combination of (M, N) is required for low PAPR.

Furthermore, the data sequence is divided into several subsequences with an equal length Len, when each subsequence employs the proposed algorithm. Fig. 10 presents the CCDF performances for various Len. The parameters are $N = 512$, $M = 32$, and $Len = 31, 63, 255$, respectively.

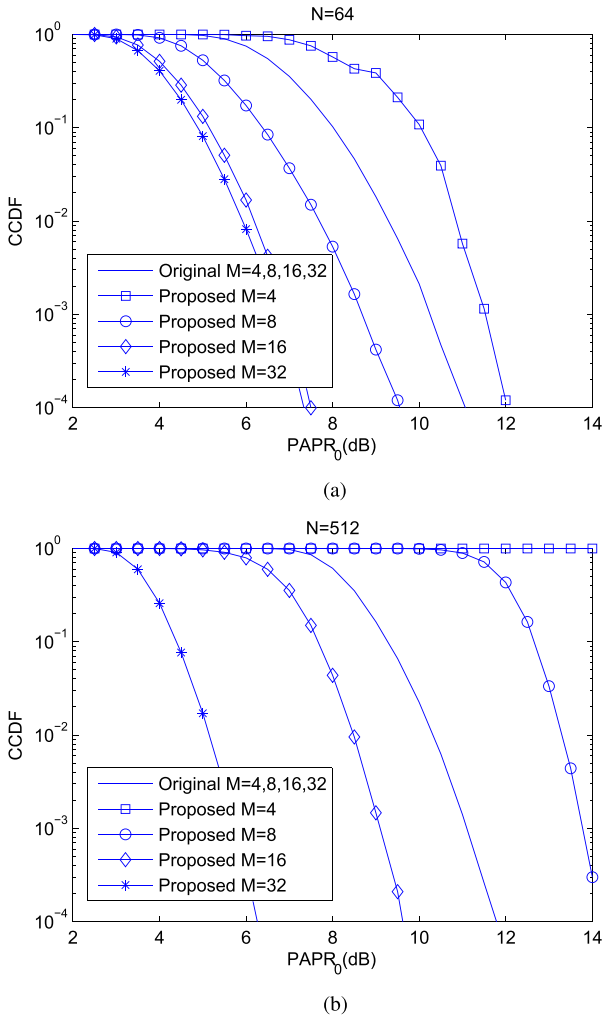

FIGURE 9. Comparison of CCDFs between the original system and the system with the proposed algorithm. $M = 4, 8, 16, 32$. (a) $N = 64$. (b) $N = 512$.

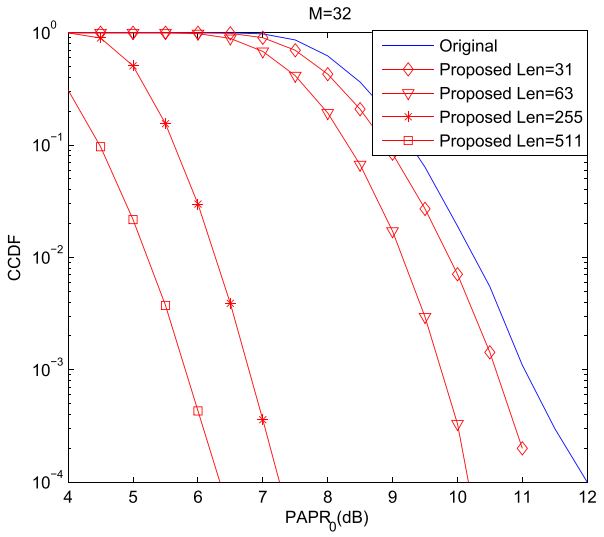

FIGURE 10. CCDFs for PAPR of the MM-DCSK system with various *Len*.

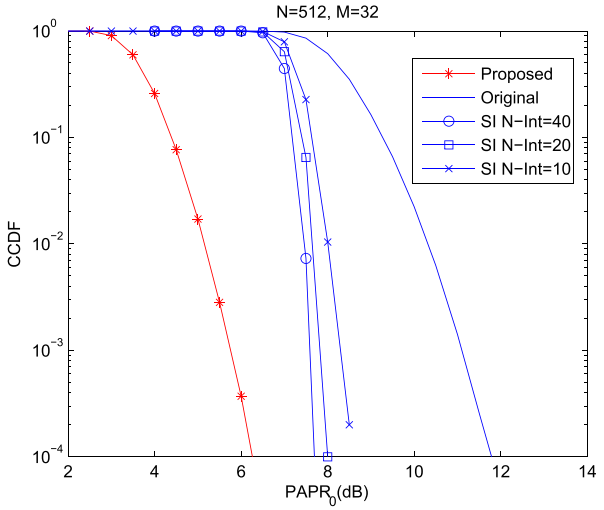

FIGURE 11. CCDFs for PAPR of the MM-DCSK system with the proposed algorithm and with the traditional SI, respectively.

It can be seen that as *Len* increases, the PAPR reduces significantly.

Fig. 11 presents the CCDF values of the MM-DCSK system with the traditional SI and the proposed algorithm, for the case of $N = 512, M = 32$. The number of interleaver (N-Int) is set to be N-Int $= 10, 20, 40$, respectively. One can observe that even by employing N-Int $= 40$, the CCDF values of the MM-DCSK system with the proposed algorithm are superior over that with the SI technique. In particular, at probability 10^{-4}, the PAPR is reduced by 5.55dB using the proposed algorithm, but only 3.1dB for the traditional SI with N-Int $= 40$.

C. PERFORMANCE COMPARISON BETWEEN MM-DCSK AND MU OFDM-DCSK SYSTEMS

The BER comparison between the proposed MM-DCSK and the MU OFDM-DCSK systems is evaluated by simulations over a three-path Rayleigh fading channel.

Since the MU OFDM-DCSK system does not support M-ary transmission, for the sake of fairness, both systems employ BPSK mapping, single user and similar bandwidths. The number of data symbol is set to be $m = 49$, the spreading factor $\beta = 64$, the FFT size $N = 128$, the maximum delays $\tau_{max} = 0.1\mu s$ and $0.2\mu s$, and the numbers of channel coefficients $P = 1, 32$, respectively.

One can observe from Fig. 12 that the performance of the MM-DCSK system is better than the MU OFDM-DCSK system for both cases of $P = 1$ and $P = 32$. Furthermore, the proposed MM-DCSK system is more robust against severe multipath effects as compared to the MU OFDM-DCSK system. For instance, when $P = 32$, the proposed MM-DCSK system outperforms the MU OFDM-DCSK system by 1dB at the value of $BER = 10^{-2}$ with $\tau_{max} = 0.1\mu s$. More significantly, for a more severe multipath scenario, i.e., $\tau_{max} = 0.2\mu s$, the performance gap increases to 7.5dB, due to the fact that the signals assigned to adjacent subcarriers have similar channel gains. On the contrary, the farther the frequency distance is, the more different the channel responses will be. Therefore, it is not easy to recover a block

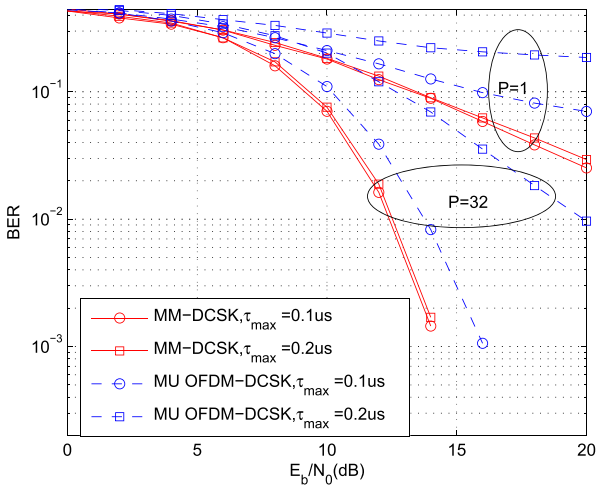

FIGURE 12. BER performance comparisons between MM-DCSK and MU OFDM-DCSK systems.

of signals by using the same reference signal for the MU OFDM-DCSK system.

V. CONCLUSION

In this paper, a multi-carrier M-ary DCSK system with a high energy efficiency and data rate is designed and analyzed, where each information signal is the reference for its next adjacent information signal, thus pilot signals are not required. Moreover, the proposed system is robust to multipath channels, which is further confirmed by comparing it with the MU OFDM-DCSK system. It is observed that, for large M, the parameter β does not have a significant impact on the BER performance, which is different from the DCSK system. Thus, the data rate can be increased by decreasing β. Another advantage of using large β is its better robustness to Doppler shift than a small one. The simulated results agree well with the analytic ones, which validates the proposed system and analysis. More importantly, it is found that repeated data symbols lead to high PAPR, while adjacent symbols with a large Euclidean distance achieve low PAPR. Accordingly, a simple PAPR-reduction algorithm is designed by rearranging the data symbols in a specific way, where only one IFFT processor is required. The simulated results show that the proposed algorithm dramatically reduces the PAPR, especially for large M. Consequently, it is concluded that the proposed MM-DCSK system is suitable for the applications that require high data rates and low-complexity devices.

REFERENCES

[1] F. C. M. Lau and C. K. Tse, *Chaos-Based Digital Communication Systems*. Heidelberg, Germany: Springer-Verlag, 2003.
[2] G. Kolumbän, B. Vizvki, W. Schwarz, and A. Abel, "Differential chaos shift keying: A robust modulation scheme for power-line communications," in *Proc. NDES*, Seville, Spain, 1996, pp. 87–92.
[3] G. Kolumbän, G. Kis, M. P. Kennedy, and Z. Jäko, "FM-DCSK: A new and robust solution to chaos communications," in *Proc. Int. Symp. Nonlinear Theory Appl.*, 1997, pp. 117–120.
[4] Y. Fang, L. Xu, L. Wang, and G. Chen, "Performance of MIMO relay DCSK-CD systems over Nakagami fading channels," *IEEE Trans. Circuits Syst. I, Reg. Papers*, vol. 60, no. 3, pp. 757–767, Mar. 2013.
[5] F. C. M. Lau, C. K. Tse, M. Ye, and S. F. Hau, "Coexistence of chaos-based and conventional digital communication systems of equal bit rate," *IEEE Trans. Circuits Syst. I, Reg. Papers*, vol. 51, no. 2, pp. 391–408, Feb. 2004.
[6] P. Chen, L. Wang, and F. C. M. Lau, "One analog STBC-DCSK transmission scheme not requiring channel state information," *IEEE Trans. Circuits Syst. I, Reg. Papers*, vol. 60, no. 4, pp. 1027–1037, Apr. 2013.
[7] W. Xu, L. Wang, and G. Chen, "Performance of DCSK cooperative communication systems over multipath fading channels," *IEEE Trans. Circuits Syst. I, Reg. Papers*, vol. 58, no. 1, pp. 196–204, Jan. 2011.
[8] S. Movassaghi, A. Majidi, A. Jamalipour, D. Smith, and M. Abolhasan, "Enabling interference-aware and energy-efficient coexistence of multiple wireless body area networks with unknown dynamics," *IEEE Access*, vol. 4, pp. 2935–2951, Jul. 2016.
[9] G. Cimatti, R. Rovatti, and G. Setti, "Chaos-based spreading in DS-UWB sensor networks increases available bit rate," *IEEE Trans. Circuits Syst. I, Reg. Papers*, vol. 54, no. 6, pp. 1327–1339, Jun. 2007.
[10] C.-C. Chong and S. K. Yong, "UWB direct chaotic communication technology for low-rate WPAN applications," *IEEE Trans. Veh. Technol.*, vol. 57, no. 3, pp. 1527–1536, May 2008.
[11] G. Kolumbän, "UWB technology: Chaotic communications versus noncoherent impulse radio," in *Proc. Eur. Conf. Circuit Theory. Design (ECCTD)*, Cork, Ireland, Aug. 2005, pp. 79–82.
[12] G. Kaddoum, E. Soujeri, and Y. Nijsure, "Design of a short reference noncoherent chaos-based communication systems," *IEEE Trans. Commun.*, vol. 64, no. 2, pp. 680–689, Feb. 2016.
[13] G. Kis, "Performance analysis of chaotic communications systems," PhD dissertation, Dept. Technol. Econom. Budpest Univ., Budpest, Hungary, Feb. 2005.
[14] T. T. Huang, L. Wang, W. Xu, and F. C. M. Lau, "Multilevel code-shifted differential-chaos-shift-keying system," *IET Commun.*, vol. 10, no. 10, pp. 1189–1195, Jul. 2016.
[15] H. Yang, W. K. S. Tang, G. Chen, and G.-P. Jiang, "System design and performance analysis of orthogonal multi-level differential chaos shift keying modulation scheme," *IEEE Trans. Circuits Syst. I, Reg. Papers*, vol. 63, no. 1, pp. 146–156, Jan. 2016.
[16] W. K. Xu, L. Wang, and G. Kolumbán, "A novel differential chaos shift keying modulation scheme," *Int. J. Bifurcation Chaos*, vol. 21, no. 3, pp. 799–814, 2011.
[17] W. K. Xu, L. Wang, and G. Kolumbän, "A new data rate adaption communications scheme for code-shifted differential chaos shift keying modulation," *Int. J. Bifurcation Chaos*, vol. 22, no. 8, pp. 1–8, Aug. 2012.
[18] S. Wang and X. Wang, "M-DCSK based chaotic communications in MIMO multipath channels with no channel state information," *IEEE Trans. Circuits Syst. II, Exp. Briefs*, vol. 57, no. 12, pp. 1001–1005, Dec. 2010.
[19] G. Cai, Y. Fang, G. Han, F. C. M. Lau, and L. Wang, "A square-constellation-based M-Ary DCSK communication system," *IEEE Access*, vol. 4, pp. 6295–6303, Sep. 2016.
[20] L. Wang, G. F. Cai, and G. Chen, "Design and performance analysis of a new multiresolution M-Ary differential chaos shift keying communication system," *IEEE Trans. Wireless Commun.*, vol. 14, no. 9, pp. 5197–5208, Sep. 2015.
[21] G. Kaddoum, F. Richardson, and F. Gagnon, "Design and analysis of a multi-carrier differential chaos shift keying communication system," *IEEE Trans. Commun.*, vol. 61, no. 8, pp. 3281–3291, Aug. 2013.
[22] H. Yang, W. K. S. Tang, G. Chen, and G.-P. Jiang, "Multi-carrier chaos shift keying: System design and performance analysis," *IEEE Trans. Circuits Syst. I, Reg. Papers*, vol. 64, no. 8, pp. 2182–2194, Aug. 2017.
[23] S. Li, Y. Zhao, and Z. Wu, "Design and analysis of an OFDM-based differential chaos shift keying communication system," *J. Commun.*, vol. 10, no. 3, pp. 199–205, 2015.
[24] G. Kaddoum, "Design and performance analysis of a multiuser OFDM based differential chaos shift keying communication system," *IEEE Trans. Commun.*, vol. 64, no. 1, pp. 249–260, Jan. 2016.
[25] Y. Rong, S. A. Vorobyov, and A. B. Gershman, "Adaptive OFDM techniques with one-bit-per-subcarrier channel-state feedback," *IEEE Trans. Commun.*, vol. 54, no. 11, pp. 1993–2003, Nov. 2006.
[26] X. Zhu and J. Xue, "On the correlation of subcarriers in grouped linear constellation precoding OFDM systems over frequency selective fading," in *Proc. VTC*, 2006, pp. 1431–1435.
[27] S. Mazahir and S. A. Sheikh, "On companding schemes for PAPR reduction in OFDM systems employing higher order QAM," *IEEE Trans. Broadcast.*, vol. 62, no. 3, pp. 716–726, Jan. 2016.

[28] A. D. S. Jayalath and C. Tellambura, "Reducing the peak-to-average power ratio of orthogonal frequency division multiplexing signal through bit or symbol interleaving," *IEE Electr. Lett.*, vol. 36, pp. 1161–1163, Jun. 2000.
[29] C. Tellambura, "Upper bound on peak factor of N-multiple carriers," *Electron. Lett.*, vol. 33, no. 19, pp. 1608–1609, Sep. 1997.

TINGTING HUANG received the B.S. degree in automation from the Wuhan University of Technology, Wuhan, China, in 2008, and the M.Sc. degree in control theory and control engineering from Fuzhou University, Fuzhou, in 2012. She is currently pursuing the Ph.D. degree with the Department of Communication Engineering, Xiamen University, Fujian, China. Her research interests include chaos-based digital communications and their applications to wireless communication.

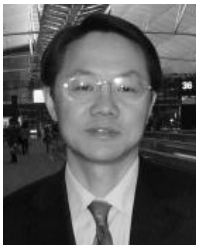

LIN WANG (S'99–M'03–SM'09) received the Ph.D. degree in electronics engineering from the University of Electronic Science and Technology of China, China, in 2001. From 1984 to 1986, he was a Teaching Assistant with the Mathematics Department, Chongqing Normal University. From 1989 to 2002, he was a Teaching Assistant, a Lecturer, and then an Associate Professor in applied mathematics and communication engineering with the Chongqing University of Post and Telecommunication, China. From 1995 to 1996, he spent one year with the Mathematics Department, University of New England, Australia. In 2003, he spent three months as a Visiting Researcher with the Center for Chaos and Complexity Networks, Department of Electronic Engineering, City University of Hong Kong. In 2013, he was a Senior Visiting Researcher with the Department of ECE, UC Davis. From 2003 to 2012, he was a Full Professor and an Associate Dean with the School of Information Science and Technology, Xiamen University, China. He has been a Distinguished Professor since 2012. He has published over 100 journal and conference papers. He holds 14 patents in physical layer in digital communications. His current research interests are channel coding, joint source and channel coding, chaos modulation, and their applications to wireless communication and storage systems.

WEIKAI XU (S'10–M'12) received the B.S. degree in electronic engineering from the Chongqing Three Gorges College, Chongqing, China, in 2000, the M.Sc. degree in communication engineering from the Chongqing University of Posts & Telecommunications, Chongqing, in 2003, and the Ph.D. degree in electronics engineering from Xiamen University, Xiamen, China, in 2011. From 2003 to 2012, he was a Teaching Assistant and an Assistant Professor in communication engineering with Xiamen University. He is currently an Associate Professor in communication engineering, Xiamen University. His research interests include channel coding, cooperative communications, chaotic communications, and ultrawideband.

GUANRONG (RON) CHEN (M'89–SM'92–F'97) has been a Chair Professor and the Director of the Centre for Chaos and Complex Networks with the City University of Hong Kong since 2000, prior to which, he was a Tenured Full Professor with the University of Houston, Houston, TX, USA. He is a member of the Academy of Europe and a fellow of The World Academy of Sciences. He received the 2011 Euler Gold Medal, Russia, and conferred Honorary Doctorate by Saint Petersburg State University, Russia, in 2011, and by the University of Le Havre, France, in 2014.